AIP | Applied Physics Letters

22.5% efficient silicon heterojunction solar cell with molybdenum oxide hole collector

Jonas Geissbühler, Jérémie Werner, Silvia Martin de Nicolas, Loris Barraud, Aïcha Hessler-Wyser, Matthieu Despeisse, Sylvain Nicolay, Andrea Tomasi, Bjoern Niesen, Stefaan De Wolf, and Christophe Ballif

Citation: Applied Physics Letters **107**, 081601 (2015); doi: 10.1063/1.4928747
View online: http://dx.doi.org/10.1063/1.4928747
View Table of Contents: http://scitation.aip.org/content/aip/journal/apl/107/8?ver=pdfcov
Published by the AIP Publishing

22.5% efficient silicon heterojunction solar cell with molybdenum oxide hole collector

Jonas Geissbühler,[1,a)] Jérémie Werner,[1] Silvia Martin de Nicolas,[1] Loris Barraud,[2] Aïcha Hessler-Wyser,[1] Matthieu Despeisse,[2] Sylvain Nicolay,[2] Andrea Tomasi,[1] Bjoern Niesen,[1] Stefaan De Wolf,[1] and Christophe Ballif[1,2]
[1]*Photovoltaics and Thin Film Electronics Laboratory, Institute of Microengineering (IMT), École Polytechnique Fédérale de Lausanne (EPFL), Rue de la Maladière 71b, CH-2000 Neuchâtel, Switzerland*
[2]*CSEM PV-Center, Jaquet-Droz 1, CH-2000 Neuchâtel, Switzerland*

(Received 6 June 2015; accepted 7 July 2015; published online 24 August 2015)

Substituting the doped amorphous silicon films at the front of silicon heterojunction solar cells with wide-bandgap transition metal oxides can mitigate parasitic light absorption losses. This was recently proven by replacing p-type amorphous silicon with molybdenum oxide films. In this article, we evidence that annealing above 130 °C—often needed for the curing of printed metal contacts—detrimentally impacts hole collection of such devices. We circumvent this issue by using electrodeposited copper front metallization and demonstrate a silicon heterojunction solar cell with molybdenum oxide hole collector, featuring a fill factor value higher than 80% and certified energy conversion efficiency of 22.5%. © *2015 AIP Publishing LLC*.
[http://dx.doi.org/10.1063/1.4928747]

The current record energy conversion efficiency for crystalline silicon (c-Si) solar cells is 25.6%, which was achieved with silicon heterojunction (SHJ) technology.[1] This device featured interdigitated contacts at the back, which offers ultimate freedom in optical optimization at the front but adds processing complexity at the back.[2,3] This is in contrast to the most simple "standard" SHJ design, where electron and hole collection is realized at opposite sides of the c-Si wafer.[4] In this way, device fabrication only relies on a few well-established processing steps without requiring patterning: Electron and hole collection is achieved by blanket n- and p-type amorphous silicon films [a-Si:H(n)/a-Si:H(p)], respectively. For improved interface passivation—essential to yield high operating voltages—thin intrinsic a-Si:H(i) films are inserted underneath these carrier-collecting films.[5,6] The doped a-Si:H layers are capped by transparent conductive oxides (TCO) on both device sides for efficient contact formation, to transport laterally the charge carriers, and to maximize light coupling into the silicon substrate.[7,8] Finally, a metal grid is usually printed or electroplated at the front for external current collection.[9]

In this simple design, for ultimate device performance, the front contact should be broadband transparent. However, due to the relatively narrow bandgap of a-Si:H of ~1.6–1.8 eV and the high defect density within the doped layer, important parasitic light absorption occurs in the ultraviolet and visible range of the solar spectrum.[10] Alternative Si-based materials with wider bandgap, such as a-SiO_x:H, μc-SiO_x:H, or a-SiC_x:H, were proposed to overcome this issue.[11,12] Unfortunately, proven optical gains for these materials bring along lowered electrical performance due to the increased band offsets at the amorphous/crystalline silicon interface, hindering efficient carrier extraction.[13–15] Even more important optical gains may be achieved by using highly transparent transition metal oxides as window layers, provided their work function is appropriate for carrier collection.[16,17] Metal oxides, and in particular, sub-stoichiometric molybdenum oxide (MoO_x, $x < 3$), were already investigated as hole collecting materials for organic[18–20] and inorganic[21–23] thin-film solar cells, as well as for organic light emitting diodes.[26–28] For these applications, the metal oxide layer often also protects sensitive underlying layers from sputtering-induced damage during TCO deposition.[24,25,29,30] Exploiting their bandgap of ~3 eV, MoO_x films were recently also integrated into SHJ devices to replace the a-Si:H(p) layers, resulting in clear optical gains.[31] However, the fill factor (*FF*) of these devices remained below 70%, with increasingly pronounced S-shaped illuminated *J-V* curves when increasing the MoO_x film thickness, indicating a hole collection issue,[31] despite its argued appropriate work function.[32,33]

Importantly, MoO_x films are sensitive to air and oxygen exposure, as well as to temperature or plasma treatments, which might impact solar cell performance.[34] Motivated by this, we present in this work a detailed investigation of the interactions between MoO_x and the layers it shares an interface with the SHJ devices (i.e., the intrinsic a-Si:H buffer layer and the TCO at the front). We demonstrate that with well-engineered processes, efficient hole collection can be obtained with such a contact, enabling measured *FF* values above 80% in SHJ solar cells.

We processed MoO_x-based as well as reference SHJ solar cells [featuring a standard a-Si:H(p) layer] as follows: First, high quality 4 Ω·cm, 230 μm n-type float-zone Si(100) wafers were etched in potassium hydroxide to obtain a random-pyramid surface texture. After chemical cleaning, the wafers were dipped in 5% hydrofluoric acid for 1 min to remove the chemically grown surface oxide. Thin intrinsic a-Si:H films were then deposited by plasma-enhanced

a)Author to whom correspondence should be addressed. Electronic mail: jonas.geissbuehler@epfl.ch

chemical vapor deposition (PECVD) on both sides of the wafer to enable high-quality interface passivation. The electron collector was realized by subsequent deposition of a thin a-Si:H(n) layer at the rear side. For hole collection, either a ~7-nm-thick thermally evaporated MoO_x or a ~6-nm-thick PECVD a-Si:H(p) layer (for the reference cells) was used on the wafer front side. All PECVD layers were deposited in an Octopus I reactor from INDEOtec SA. More details on the a-Si:H and MoO_x film depositions can be found elsewhere.[31,35] A ~65-nm-thick hydrogenated indium oxide/indium tin oxide (IO:H/ITO) bi-layer was deposited as front-TCO by RF/DC magnetron sputtering (MRC 603).[36] The back electrode was realized by an ITO/Ag stack deposited in the same sputtering setup. Finally, a low-temperature silver paste was screen-printed to form the front grid, followed by curing (<200 °C). The optical absorptance of MoO_x, a-Si:H, and TCO films was measured with a spectrophotometer (Lambda 950, Perkin Elmer) fitted with an integrating sphere on co-deposited AF32 glass witness samples. The annealing of these films was carried in a N_2 purged oven. Film thicknesses on these planar substrates are 1.7 times higher than for layers deposited on random-pyramid textured c-Si wafers due to deposition directionality.[37] High-resolution transmission electron microscopy (HR-TEM) was carried out on selected samples using a FEI Osiris instrument. For this, cross-section samples were prepared using mechanical tripod polishing (Allied High Tech Multiprep) followed by low-energy Ar ion milling (Gatan PIPS). Finally, completed solar cells were characterized by light *J-V* (Wacom solar simulator, Keithley 2601A sourcemeter) and external quantum efficiency (EQE, in-house built setup).

To illustrate the influence of subsequent processing steps on the optical properties of the MoO_x layer, Fig. 1(a) shows the optical absorptance of device-relevant MoO_x and IO:H/ITO films on glass prior to annealing, either deposited *separately* or *sequentially* (IO:H/ITO bilayer sputtered on MoO_x film). Absorptance spectra of a-Si:H(p) and of bare AF32 glass substrates are also provided for reference. In the as-deposited state [see panel (a)], as a result of its ~3 eV bandgap, the MoO_x spectrum features a cut-off wavelength at 400 nm, while the absorptance in the visible and infrared ranges remains below 2%. The same graph also shows the absorptance of the IO:H/ITO bilayer (deposited at room temperature) used here as highly transparent TCO. Surprisingly, when MoO_x is capped with this IO:H/ITO bilayer, the total absorptance is significantly higher than expected from the spectra of the individual layers.[25] Increased absorptance of MoO_x is known to result from low-temperature annealing in N_2 atmosphere [see also Fig. 1(b)], which can be explained by an increase of oxygen vacancies in this material.[38,39] In our case, sputtering takes place at a temperature below 50 °C and can therefore not explain these optical changes. Exposing our MoO_x films directly to a pure Ar plasma revealed that the increased absorptance is induced both by bombardment with energetic particles and by plasma UV luminescence, causing photochromism of MoO_x.[30,40] When subsequently annealed, changes in the optical properties of the MoO_x/TCO layer stack are mainly due to the crystallization of the TCO, as seen by the blue-shift of the cut-off and decreased free carrier absorption in the infrared.[41] Additional investigations revealed that the nature of the annealing atmosphere (reducing or oxidizing) has no impact on the optical properties of the MoO_x/IO:H/ITO stack (data not shown). We attribute this to the efficient capping provided by the TCO bi-layer.[36]

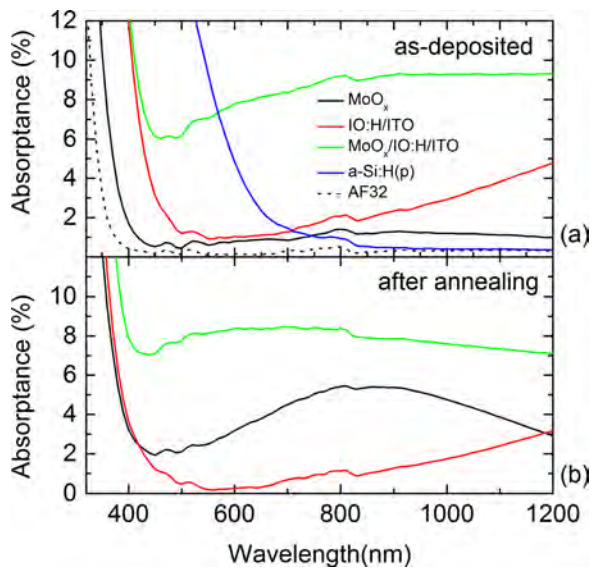

FIG. 1. Optical absorptance of MoO_x films and IO:H/ITO bilayers deposited separately or sequentially on AF32 glass (a) before and (b) after 200 °C annealing (in N_2 for 25 min). Absorptance spectra of a thin a-Si:H(p) film and of bare AF32 glass are given for reference.

To further investigate the MoO_x/TCO interaction and its evolution during annealing, HR-TEM was carried out on mirror-polished c-Si samples, capped with a full a-Si:H(i)/MoO_x/IO:H/ITO contact stack. Figures 2(a) and 2(b) show such a stack in its as-deposited and annealed states (25 min at 200 °C in a N_2 purged oven), respectively. In either case, an atomically sharp and defect-free c-Si/a-Si:H(i) interface is seen, required for high-quality surface passivation.[42] Similarly, the a-Si:H(i)/MoO_x interface is clearly delimited. In contrast, the MoO_x/IO:H interface is less sharply resolved, suggesting the presence of a ~1–2 nm-thick intermixing layer induced by the sputtering process [Fig. 2(a)].

Panel (b) indicates that during annealing, the presence of this intermixing layer becomes more pronounced and reaches a thickness of 5–7 nm with the occurrence of epitaxial nano-grains on the IO:H lattice [Fig. 2(b), indicated by the white arrow].

Next, we investigated the impact of the presence of the MoO_x layer and the subsequent annealing on the passivation properties of the a-Si:H(i) buffer layer. For this, we evaluated the effective minority carrier lifetime (τ_{eff}) of the silicon wafer by transient photoconductance measurements (Sinton Instruments, WCT-120),[43,44] which gives direct information on the surface passivation quality. Figure 3(a) shows τ_{eff} (at a carrier injection level of 10^{15} cm^{-3}) as a function of the annealing time (at 200 °C in a N_2 environment). Both passivation samples (with and without MoO_x overlayer) increase their τ_{eff} within the first minutes of annealing, which is explained by a reorganization of the passivating film's microstructure.[45,46] However, for longer annealing, τ_{eff} slightly decays for the MoO_x sample. Similar annealing effects were observed in the past when capping a-Si:H(i) buffer layers with p-type a-Si:H films, which was explained

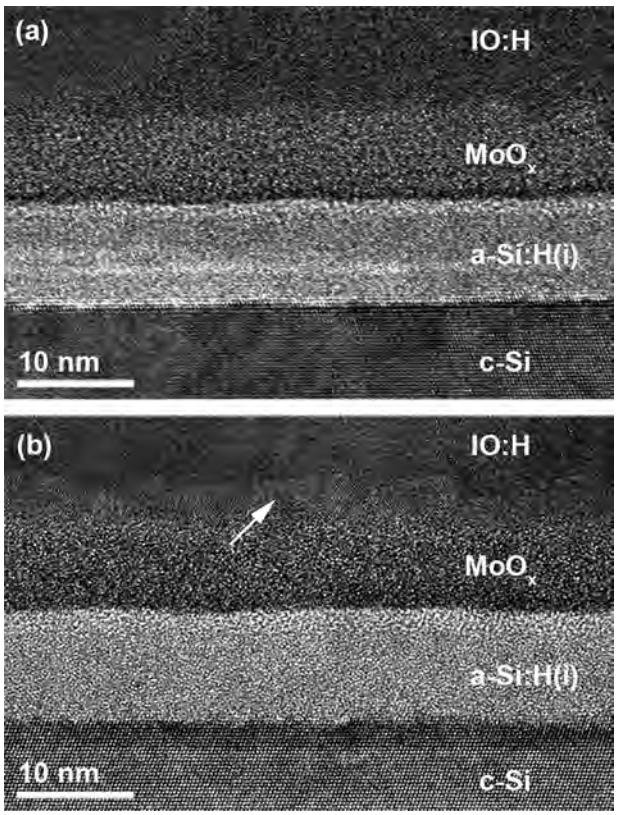

FIG. 2. HR-TEM micrographs of the c-Si/a-Si:H(i)/MoO$_x$/IO:H interfaces for (a) an as-deposited sample and (b) after annealing at 200 °C in N_2 for 25 min. Images are purposely defocused to increase the contrast of the MoO$_x$/IO:H interfacial layer.

by Fermi-level induced native defect generation in the passivating films.[47] Here, the magnitude of this effect remains modest, as seen in Fig. 3(b), where τ_{eff} is increased for all injection levels excluding any negative effect on device performance.

Summarizing our findings so far, we conclude that (1) oxygen vacancies are created in the MoO$_x$ film by the TCO deposition process; (2) subsequent annealing may result in the formation of an interlayer between MoO$_x$ and IO:H; (3) the annealing required for the Ag paste curing does not alter markedly the passivation properties of the a-Si:H(i) buffer layer.

To investigate the impact of annealing on device level, we fabricated solar cells featuring either MoO$_x$ or standard a-Si:H(p) hole extraction layers. The cells were metallized by using screen-printing, followed by annealing at the lowest possible temperature to evaporate the solvents contained within the silver paste. This pre-drying is mandatory to obtain a reasonable electrical conductivity and mechanical stability and was carried at 100 °C for 25 min (instead of the typically used 200 °C for 25 min). Once finished, the cells were subsequently annealed at 130 °C, 180 °C, and 200 °C in steps of 15 min. For the reference cell, Fig. 4(a) confirms that increasing the annealing temperature up to 200 °C improves the device performance (*FF* improves from 75.4% to 77.1%), linked to the improved metal conductivity as well as to improved passivation (seen also in Fig. 3).[48] In contrast to this, Fig. 4(b) shows that annealing above 130 °C dramatically deteriorates the performances of our MoO$_x$-based cell.[16] The *J-V* characteristics become S-shaped (*FF* deteriorates from 76.6% to 69.7%), strongly suggesting the appearance of a hole-blocking barrier. A possible cause for this barrier is the earlier discussed MoO$_x$/TCO interlayer, which thickens with annealing. However, an exhaustive characterization of the interlayer film composition remains necessary to fully establish this view. The occurrence of the S-shaped curves was found to be independent of the annealing ambient (air or N_2-purged, data not shown). Hence, processing above 130 °C temperature must be avoided to preserve efficient hole collection. In addition, we note that the J_{SC} remains unchanged after annealing as the decreased absorptance in the 650–1200 nm range is counterbalanced by losses in the 400–650 nm range accordingly to Fig. 1.

We now directly compare MoO$_x$-based and reference devices. Figure 5 shows both cell structures featuring identical TCO layers (IO:H/ITO bilayer), but annealed at their respective optimal conditions (namely, 100 °C for the MoO$_x$-based cell and 200 °C for the reference device). Focusing on the solar-spectrum integrated EQE curves, we see a substantial gain of 0.88 mA cm^{-2} in the 310–610 nm wavelength range for the MoO$_x$-based device. However, this gain is partially lost by parasitic light absorption, caused by the MoO$_x$/TCO interaction, and by the lower optical transparency of non-cured IO:H/ITO films (Fig. 1). At 800 nm, the EQE of the MoO$_x$-based cell is 2% absolute lower than

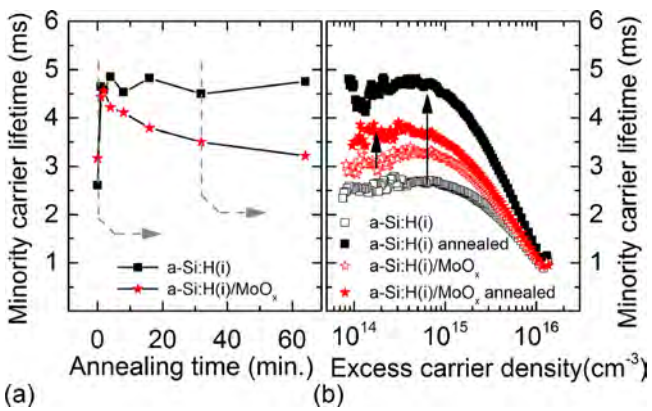

FIG. 3. (a) Minority carrier lifetime at an injection level of 10^{15} cm^{-3} as a function of the sample annealing time. (b) Minority carrier lifetime curves in function of the injection level before and after a 32 min annealing.

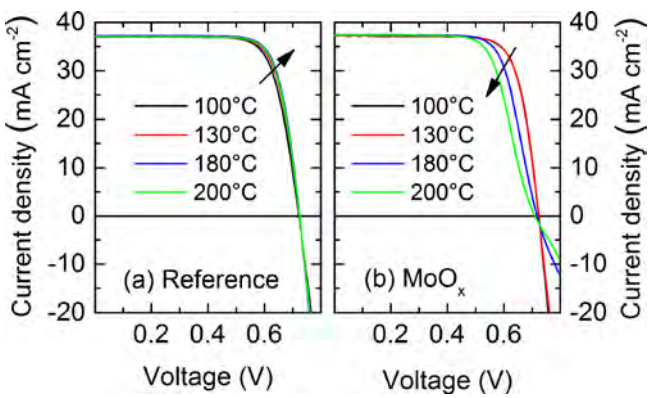

FIG. 4. Light *J-V* characteristics of (a) reference and (b) MoO$_x$-based SHJ solar cells after post-processing annealing at various temperatures. Measurements were taken at room temperature.

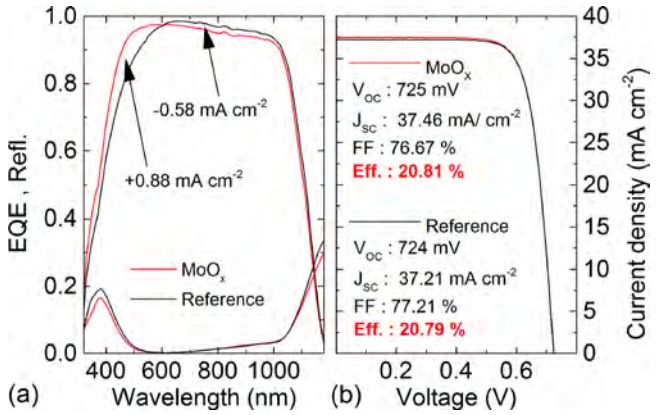

FIG. 5. (a) EQE and (b) light *J-V* characteristic of MoO_x-based and a-Si:H(p) references SHJ solar cells with adapted silver paste curing temperature.

its reference counterpart. This difference is actually smaller than expected from the data in Fig. 1, which can be explained by the 1.7 thinner layers in our devices, compared to test structures shown in Fig. 1. These detrimental effects lead to a 0.58 mA cm^{-2} loss for wavelengths above 610 nm. We note that despite different refractive indices, both a-Si:H(p) and MoO_x devices present similar reflectance characteristics.[49] This was confirmed by optical simulations where only a ~1% difference was obtained due to the extremely thin films considered here. Consequently, the illuminated *J-V* curve of the MoO_x-based cell shows a ~0.3 mA cm^{-2} total gain in short-circuit current density (J_{SC}).

As already pointed out, key to our results is the avoidance of post-deposition processes above 130 °C. With this, the presented MoO_x-cell has a significantly better *FF* than the one obtained in the earlier studies, reaching now values on par with standard SHJ cells.[31] This underlines that MoO_x can be an efficient hole collector, also at standard operating temperatures.[50] The discrepancy between the J_{SC} of the present study and the one obtained by Battaglia *et al.* is two-fold: First, a-Si:H(i) layers with different thicknesses were used, which can lead to a J_{SC} difference up to 1 mA cm^{-2}.[10] Second, the IO:H was not annealed in our case leading to more parasitic light absorption in the blue part of the spectrum accordingly to Fig. 1.[31]

Finally, we discuss how the thermal processing limitation for these devices does not exclude ultimate device performance. In this context, a significant improvement can be achieved by replacing the Ag-printed metallization by Cu electrodeposition, not requiring any thermal treatment. Furthermore, this process reduces substantially the finger width (20 μm, compared to 70–80 μm for screen-printing), reducing optical shadowing from 5%–7% down to 2%–3% while increasing the number of finger from 9 to 20.[9] To test this in MoO_x-based devices, we first deposited a ~30-nm-thick Cu seed layer on the front TCO by thermal evaporation (Leybold Vacuum), which was selectively masked by a photolithographically patterned resist. In the unmasked areas, the Cu was then thickened by electrodeposition at room-temperature, in a home-built system using a Cu sulfate electrolyte. Finally, after photoresist removal, the seed-layer between the fingers was removed in 1 min in a basic Cu etchant at room temperature.[9,51] Using this modified metallization scheme, the *FF* of the finished device is significantly increased up to 80.36%, as can be deduced from the illuminated *J-V* characteristics given in Fig. 6. This is explained by a lower line resistivity in the Cu electrodeposited front-grid compared to the screen-printed cells previously presented, corresponding to a reduction in series resistance from 1.62 to 0.83 $\Omega \cdot cm^2$. Moreover, the overall front-grid shadowing is reduced compared to screen-printed cell, resulting in an additional J_{SC} gain.[9]

With these *FF* and J_{SC} improvements, while maintaining a similar open-circuit voltage (V_{OC}), we obtained an energy-conversion efficiency of 22.5% for a 4 cm^2 solar cell certified by the Fraunhofer ISE CalLab (Fig. 6). Further simple improvements can be made in the optical design of the cell. For this, the TCOs relying on a thermal treatment for crystallization (as the IO:H/ITO bilayer used in the present study) can be replaced by amorphous TCOs, which do not require any annealing to tune the optical and electrical properties.[52] Furthermore, by replacing IO:H, the sputtering process would not rely on water vapor as a dopant source, which simplifies the process and avoids possible water-MoO_x interactions.

In summary, we showed that when replacing the p-type amorphous silicon film with a MoO_x layer at the front of SHJ solar cells, the properties of the MoO_x layer are strongly impacted by subsequent processing steps. Specifically, sputtering of the TCO leads to increased light absorption, likely due to an increased oxygen vacancy density within the MoO_x film. However, this effect was not found to be detrimental for the electrical cell performance. In addition, processes above 130 °C significantly increase the thickness of the MoO_x/IO:H interfacial layer and possibly be the cause of the hole-blocking behavior and *FF* loss observed when devices are annealed above this temperature. Therefore, by maintaining all processes below this temperature, similar performances as those for a a-Si:H(p) reference SHJ solar cell can be obtained, despite suboptimal material properties. In this respect, specific processes specially designed for low temperatures significantly improve cell performance, such that an energy conversion efficiency of 22.5% is demonstrated with copper-plated front metallization. These results therefore demonstrate that metal oxide layers can be used as a

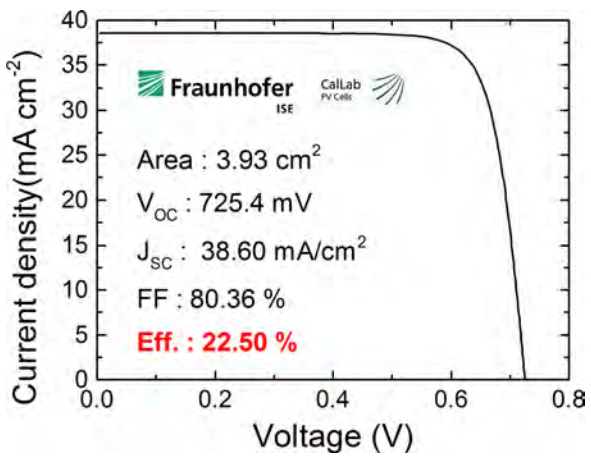

FIG. 6. Light *J-V* characteristic of MoO_x-based SHJ solar cells with Cu electrodeposited front grid (certified by the Fraunhofer ISE CalLab).

replacement for p-doped amorphous silicon layers in highly efficient SHJ cells, improving optical performance while maintaining excellent passivation and high fill factors.

The authors gratefully acknowledge Danièle Laub and Colette Valloton of CIME for HR-TEM sample preparation; Cédric Bucher, Lionel Domon, Nicolas Badel, Niels Holm, and Joël Currit for their technical support; Fabien Debrot, Christophe Allebé, and Derk Baetzner for wafer preparation; Johannes Seif, James Bullock, Laura Ding, Mathieu Boccard, and Monica Morales-Masis for fruitful discussions; and Yannick Riesen and Anna Jungbluth for their support in sample characterization. This work was supported by European Community's FP7 Program under the Hercules project (Contract No. 608498) and CHEETAH project (Contract No. 609788), the Swiss Commission for Technology and Innovation under the TACOS project (No. 16637.2 PFNM-NM), the Axpo Naturstrom Fonds Switzerland, the CCEM connect PV project, the DOE under the FPaceII project (No. DE-EE0006335), the EuroTech Universities Alliance, and by the Swiss Federal Office for Energy (SFOE).

[1]K. Masuko, M. Shigematsu, T. Hashiguchi, D. Fujishima, M. Kai, N. Yoshimura, T. Yamaguchi, Y. Ichihashi, T. Mishima, N. Matsubara, T. Yamanishi, T. Takahama, M. Taguchi, E. Maruyama, and S. Okamoto, IEEE J. Photovoltaics **4**, 1433–1435 (2014).
[2]K. K. N. Koide, T. Sakai, T. Kuniyoshi, H. Katayama, N. Asano, T. Hieda, and J. Nakamura, paper presented at the 23rd Photovoltaic Specialist Conference, Taipei, Taiwan (2013).
[3]A. Tomasi, B. Paviet-Salomon, D. Lachenal, S. Martin de Nicolas, A. Descoeudres, J. Geissbühler, S. De Wolf, and C. Ballif, IEEE J. Photovoltaics **4**, 1046–1054 (2014).
[4]S. De Wolf, A. Descoeudres, Z. C. Holman, and C. Ballif, Green **2**, 7 (2012).
[5]A. Descoeudres, L. Barraud, R. Bartlome, G. Choong, S. De Wolf, F. Zicarelli, and C. Ballif, Appl. Phys. Lett. **97**, 183505 (2010).
[6]A. Descoeudres, L. Barraud, S. De Wolf, B. Strahm, D. Lachenal, C. Guerin, Z. C. Holman, F. Zicarelli, B. Demaurex, J. Seif, J. Holovsky, and C. Ballif, Appl. Phys. Lett. **99**, 123506 (2011).
[7]Z. C. Holman, A. Descoeudres, S. De Wolf, and C. Ballif, IEEE J. Photovoltaics **3**, 1243–1249 (2013).
[8]Z. C. Holman, M. Filipič, A. Descoeudres, S. De Wolf, F. Smole, M. Topič, and C. Ballif, J. Appl. Phys. **113**, 013107 (2013).
[9]J. Geissbühler, S. De Wolf, A. Faes, N. Badel, Q. Jeangros, A. Tomasi, L. Barraud, A. Descoeudres, M. Despeisse, and C. Ballif, IEEE J. Photovoltaics **4**, 1055–1062 (2014).
[10]Z. C. Holman, A. Descoeudres, L. Barraud, F. Z. Fernandez, J. P. Seif, S. De Wolf, and C. Ballif, IEEE J. Photovoltaics **2**, 7–15 (2012).
[11]K. Ding, U. Aeberhard, F. Finger, and U. Rau, J. Appl. Phys. **113**, 134501 (2013).
[12]D. Pysch, M. Bivour, M. Hermle, and S. W. Glunz, Thin Solid Films **519**, 2550–2554 (2011).
[13]J. P. Seif, A. Descoeudres, M. Filipič, F. Smole, M. Topič, Z. C. Holman, S. De Wolf, and C. Ballif, J. Appl. Phys. **115**, 024502 (2014).
[14]L. Mazzarella, S. Kirner, B. Stannowski, L. Korte, B. Rech, and R. Schlatmann, Appl. Phys. Lett. **106**, 023902 (2015).
[15]H. Fujiwara, T. Kaneko, and M. Kondo, Appl. Phys. Lett. **91**, 133508 (2007).
[16]M. Bivour, J. Temmler, H. Steinkemper, and M. Hermle, "Molybdenum and tungsten oxide: High work function wide band gap contact materials for hole selective contacts of silicon solar cells," Sol. Energy Mater. Sol. Cells (published online, 2015).
[17]C. Battaglia, X. Yin, M. Zheng, I. D. Sharp, T. Chen, S. McDonnell, A. Azcatl, C. Carraro, B. Ma, R. Maboudian, R. M. Wallace, and A. Javey, Nano Lett. **14**, 967–971 (2014).
[18]S. Chen, J. R. Manders, S. W. Tsang, and F. So, J. Mater. Chem. **22**, 24202–24212 (2012).
[19]J. Griffin, D. C. Watters, H. Yi, A. Iraqi, D. Lidzey, and A. R. Buckley, Adv. Energy Mater. **3**, 903–908 (2013).
[20]V. Shrotriya, G. Li, Y. Yao, C. W. Chu, and Y. Yang, Appl. Phys. Lett. **88**, 073508 (2006).
[21]S. Il Park, S. Jae Baik, J. S. Im, L. Fang, J. W. Jeon, and K. Su Lim, Appl. Phys. Lett. **99**, 063504 (2011).
[22]C. Gretener, J. Perrenoud, L. Kranz, C. Baechler, S. Yoon, Y. E. Romanyuk, S. Buecheler, and A. N. Tiwari, Thin Solid Films **535**, 193–197 (2013).
[23]L. Fang, S. Jae Baik, and K. Su Lim, Thin Solid Films **556**, 515–519 (2014).
[24]P. Löper, S. J. Moon, S. Martín de Nicolas, B. Niesen, M. Ledinsky, S. Nicolay, J. Bailat, J. H. Yum, S. De Wolf, and C. Ballif, Phys. Chem. Chem. Phys. **17**, 1619–1629 (2015).
[25]J. Werner, G. Dubuis, A. Walter, P. Löper, S.-J. Moon, S. Nicolay, M. Morales-Masis, S. De Wolf, B. Niesen, and C. Ballif, Sol. Energy Mater. Sol. Cells **141**, 407–413 (2015).
[26]S. Hamwi, J. Meyer, M. Kröger, T. Winkler, M. Witte, T. Riedl, A. Kahn, and W. Kowalsky, Adv. Funct. Mater. **20**, 1762–1766 (2010).
[27]J. Meyer, T. Winkler, S. Hamwi, S. Schmale, H. H. Johannes, T. Weimann, P. Hinze, W. Kowlasky, and T. Riedl, Adv. Mater. **20**, 3839–3843 (2008).
[28]J. Meyer, S. Hamwi, M. Kröger, W. Kowalsky, T. Riedl, and A. Kahn, Adv. Mater. **24**, 5408–5427 (2012).
[29]T. J. Tate, M. Garcia-Parajo, and M. Green, J. Appl. Phys. **70**, 3509 (1991).
[30]J. H. Kim, Y. J. Lee, Y. S. Jang, J. N. Jang, D. H. Kim, B. C. Song, D. H. Lee, S. N. Kwon, and M. P. Hong, Org. Electron. **12**, 285–290 (2011).
[31]C. Battaglia, S. Martin de Nicolás, S. De Wolf, X. Yin, M. Zheng, C. Ballif, and A. Javey, Appl. Phys. Lett. **104**, 113902 (2014).
[32]M. Bivour, S. Schröer, and M. Hermle, Energy Procedia **38**, 658–669 (2013).
[33]J. Bullock, A. Cuevas, T. Allen, and C. Battaglia, Appl. Phys. Lett. **105**, 232109 (2014).
[34]I. Irfan and Y. Gao, J. Photon. Energy **2**, 021213 (2012).
[35]A. Descoeudres, Z. C. Holman, L. Barraud, S. Morel, S. De Wolf, and C. Ballif, IEEE J. Photovoltaics **3**, 83–89 (2013).
[36]L. Barraud, Z. C. Holman, N. Badel, P. Reiss, A. Descoeudres, C. Battaglia, S. De Wolf, and C. Ballif, Sol. Energy Mater. Sol. Cells **115**, 151–156 (2013).
[37]S. Olibet, E. Vallat-Sauvain, L. Fesquet, C. Monachon, A. Hessler-Wyser, J. Damon-Lacoste, S. De Wolf, and C. Ballif, Phys. Status Solidi A **207**, 651–656 (2010).
[38]S. Y. Lin, Y. C. Chen, C. M. Wang, P. T. Hsieh, and S. C. Shih, Appl. Surf. Sci. **255**, 3868–3874 (2009).
[39]K. H. Wong, K. Ananthanarayanan, J. Luther, and P. Balaya, J. Phys. Chem. C **116**, 16346–16351 (2012).
[40]T. He and J. Yao, J. Photochem. Photobiol. C **4**, 125–143 (2003).
[41]T. Koida, H. Fujiwara, and M. Kondo, Jpn. J. Appl. Phys., Part 1 **46**, 685–687 (2007).
[42]J. Geissbühler, S. De Wolf, B. Demaurex, J. P. Seif, D. T. L. Alexander, L. Barraud, and C. Ballif, Appl. Phys. Lett. **102**, 231604 (2013).
[43]R. A. Sinton and A. Cuevas, Appl. Phys. Lett. **69**, 2510–2512 (1996).
[44]H. Nagel, C. Berge, and A. G. Aberle, J. Appl. Phys. **86**, 6218 (1999).
[45]S. De Wolf, S. Olibet, and C. Ballif, Appl. Phys. Lett. **93**, 032101 (2008).
[46]E. M. El Mhamdi, J. Holovsky, B. Demaurex, C. Ballif, and S. De Wolf, Appl. Phys. Lett. **104**, 252108 (2014).
[47]S. De Wolf and M. Kondo, J. Appl. Phys. **105**, 103707 (2009).
[48]B. Demaurex, S. De Wolf, A. Descoeudres, Z. C. Holman, and C. Ballif, Appl. Phys. Lett. **101**, 171604 (2012).
[49]R. Liu, S.-T. Lee, and B. Sun, Adv. Mater. **26**, 6007–6012 (2014).
[50]This was further evidenced by temperature-dependent light *J-V* measurements in which an equivalent energy-conversion temperature coefficient of −0.235%/°C was measured for both MoO_x- and reference-cells.
[51]W. P. Mulligan *et al.*, "Solar cell and method of manufacture," U.S. patent US7897867 B1 (1 March 2011).
[52]M. Morales-Masis, S. Martin de Nicolas, J. Holovsky, S. De Wolf, and C. Ballif, "Low-Temperature High-Mobility Amorphous IZO for Silicon Heterojunction Solar Cells," IEEE J. Photovoltaics (published online, 2015).